Supporting Information

Salts Induce Enhanced Disintegration of Natural Minerals in Charged Water Microdroplets

*Jamshiya Sulthana,[‡a] Anubhav Mahapatra,[‡a] Mridula Bhan,[a] Depanjan Sarkar[*ac] and Thalappil Pradeep[*abc]*

[a]DST Unit of Nanoscience (DST UNS) & Thematic Unit of Excellence (TUE), Department of Chemistry, Indian Institute of Technology Madras (IITM), Chennai - 600036, India.

[b]International Centre for Clean Water, 2nd Floor, B-Block, IIT Madras Research Park, Kanagam Road, Taramani, Chennai - 600113, India.

[c]Centre of Excellence on Molecular Materials and Functions, Department of Chemistry, Indian Institute of Technology Madras, Chennai – 600036, India.

***Corresponding author:**

Depanjan Sarkar, Email id: depanjan_coe@icsrpis.iitm.ac.in

Thalappil Pradeep, Email id: pradeep@iitm.ac.in

Table of contents

S1. Materials

All reagents were obtained from commercial suppliers and used as received, without further purification. The materials employed in this study include sodium chloride (NaCl ≥ 99.0 %, Merck Specialities Pvt. Ltd.), silicon dioxide (SiO_2 - natural quartz), hydrochloric acid (HCl, Merck Specialities Pvt. Ltd.), lithium chloride (LiCl, Merck Specialities Pvt. Ltd.), potassium chloride (KCl, Merck Specialities Pvt. Ltd.), rubidium chloride (RbCl, Sisco Research Laboratories Pvt. Ltd.), cesium chloride (CsCl, Sisco Research Laboratories Pvt. Ltd.), sodium fluoride (NaF, Sisco Research Laboratories Pvt. Ltd.), sodium bromide (NaBr, Sisco Research Laboratories Pvt. Ltd.), and sodium iodide (NaI, Sisco Research Laboratories Pvt. Ltd.).

Quartz was extracted from river sand, thoroughly washed with deionized water to remove impurities, dried, and ground into fine powder using an mortar and pestle. Ultrapure water (resistivity = 18.2 MΩ·cm, Millipore Milli-Q System, India) was used throughout all experiments with spiking different salts in it.

S2. Experimental Methods

S2.1. Preparation of suspension of quartz

River sand was first washed multiple times with deionized water, dried, and sieved to isolate quartz particles. The quartz was finely ground using a mortar and pestle. Approximately 10 mg of quartz powder was suspended in 2 mL of Milli-Q water, followed by ultrasonication for 2 minutes to achieve uniform dispersion. The suspension was centrifuged at 1000 rpm for 1 minute to remove large particulates. The supernatant was collected and ultrasonicated again for 2 minutes, followed by sequential centrifugation at 15,000 rpm to separate the desired particle size and ultra-fine nanoparticles (which stay in the supernatant). The fraction produced as precipitate (~ 0.4 mg) in 5–10 μm as shown in Figure S1 was retained and re-suspended for subsequent salt addition and electrospray experiments.

S2.2. Preparation of NaCl Stock Solutions

A stock solution of NaCl (5 mg/mL) was prepared by dissolving 5 mg NaCl (≥ 99 %) in 1 mL of Milli-Q water and ultrasonicated to ensure complete dissolution. 10 μL of the prepared solution was diluted in 990 μL of water to obtain a 0.05 mg/mL solution consisting NaCl in it. Serial dilutions were then performed to obtain concentrations corresponding to 5 ppm (85.6 μM), 0.5 ppm (8.56 μM), 0.1 ppm (1.71 μM), and 0.05 ppm (0.86 μM).

For each experiment, 0.5 mL of the desired NaCl solution was added to ~ 0.4 mg of quartz precipitate (Sample 1) to achieve the final salt concentration. Before electrospray deposition, 20 μL aliquots of each quartz-NaCl mixture were drop-casted onto an aluminum substrate and imaged with field-emission scanning electron microscopy (FESEM) to verify uniformity of micron-sized particles in the suspension, which was used further for electrospraying.

S2.3. Preparation of precursor suspension for electrospray

A 200 µL aliquot of Sample 1 was mixed with 800 µL of the respective NaCl solution to achieve the target concentration while maintaining a constant amount of quartz (~0.4 mg) in the mixture. The mixture was ultrasonicated well to ensure homogenization and loaded into a gastight Hamilton syringe (0.5 mL).

S3. Electrospray deposition experiments

A custom-built electrospray setup in Figure S2 was employed to generate charged microdroplets. A 0.5 mL gas-tight Hamilton syringe fitted with a 22-gauge needle (inner diameter 413 µm) was connected to a polyimide coated fused quartz capillary (inner diameter 50 µm, Polymicro Technologies™, Molex, USA) using a union connector. The syringe needle was connected to a high-voltage DC power supply, while the collection substrate carbon-coated copper TEM grid (300 mesh) was grounded and placed on a metal plate 1.5 cm below the capillary tip.

A stepper motor with 400 steps per revolution was used to precisely control the flow rate at 0.1 mL/h. Experiments were carried out under ambient conditions (25 °C, 50–60 % RH). Applied potentials ranged between 1.5 and 4.5 kV depending on salt concentration. PEEK tubing, ferrules, and connectors were procured from IDEX Health & Science, USA.

S4. Characterization by electron microscopy

Morphological and structural characterization was performed using Field Emission Scanning Electron Microscopy (FESEM) by Thermo Fisher Verios G4 UC operated at 10 kV and emission current of 0.10 nA. Samples were sputter-coated with ~ 0.2 nm Au using a Quorum Q150T S Plus sputter coater. Transmission Electron Microscopy (TEM) by Thermo Fisher

Talos™ F200i and operating at 200 kV was utilized. Carbon-coated copper TEM grids (300 mesh) were glow-discharged using Quorum GloQube Plus before sample deposition to enhance hydrophilicity. High-resolution Transmission electron microscopic (HRTEM) images were analyzed to determine lattice spacing, confirming the crystalline structure of the disintegrated nanoparticles of quartz.

S5. Results and Discussion

S5.1. Morphology of Pristine Quartz

Pristine quartz particles, characterized by FESEM, exhibited sizes in the range of 5–10 μm with well-defined crystalline edges (Figure S1). This confirmed the structural integrity of the particles prior to treatment of electrospray. Electrospraying quartz suspensions in ultrapure water (18 MΩ cm, Milli-Q) required an applied potential of at least 4.5 kV to achieve disintegration to form nanoparticles, consistent with earlier reports on charged water microdroplet-induced mineral weathering. Below this threshold, only micron-sized aggregates were recovered.

S5.2. Effect of equal ionic concentration on the disintegration of quartz

A controlled comparison between equal number of ions of HCl and NaCl (1.5 μM each) was performed under identical electrospray conditions (2.0 kV, 1.5 cm tip-to-substrate distance) to isolate the influence of ion type from ionic strength. Both systems produced uniform quartz nanoparticles, confirming that ion availability governs disintegration initiation. However, H^+ ions enabled disintegration at lower voltages (1.5 kV) due to proton-assisted hydrolysis and enhanced interfacial polarization, whereas Na^+ required higher fields (2.0-2.5 kV). This demonstrates that hydration strength and interfacial chemistry changes upon introduction of

different kinds of ions, rather than ionic concentration alone, dictate the energy efficiency of charged droplet-induced disintegration of quartz as shown in Figure S4.

S6. Theoretical analysis

Finite-element COMSOL static simulations were conducted for a two-phase droplet system consisting of a dielectric quartz core (ε_r = 4) surrounded by an aqueous shell (ε_r = 78-80) suspended in air (ε_r = 1). The liquid phase as a drop is held together by surface tension, which minimizes its surface area, favoring a spherical shape. When electric charge is added to the drop, it distributes on the surface, creating an outward Coulombic electrostatic force, as shown in Figure 1a. As the concentration of dissolved ions increases, this outward force increases, because of the increased charge density.

The electric displacement field norm (C/m^2) and electric field norm (V/m) both showed strong amplification at the quartz–water interface as salt concentration increased (0.1 ppm), resulting in disintegration of quartz mineral at lower applied voltage (2.5 kV).

Charge relaxation length ($\mathbf{d_m}$) was calculated using

$$dm = \left(\frac{(\gamma\tau^2)}{\rho}\right)^{1/3},$$

where γ is surface tension, τ is relaxation time (ε/K), ε is permittivity, and K is conductivity. For 0.5 ppm NaCl, τ = 0.692 s and d_m = 3.29 μm; for 0.1 ppm, τ = 2.31 s and d_m = 7.32 μm. Rapid relaxation in higher-conductivity systems favors fine droplet fission and efficient energy transfer.

S6.1. Correlation between conductivity and surface tension

Conductivity measurements showed a linear increase with NaCl concentration up to 1 ppm, while surface tension remained nearly constant as shown in Figure S5 The combination of enhanced conductivity and minimal surface tension alteration promotes stable, charge-rich microdroplets that can efficiently disintegration of quartz at lower voltages.

The Rayleigh limit defines the critical point where the electrostatic forces exactly balance the cohesive force induced by inherent surface tension. Beyond this limit, the drop becomes unstable and must shed charge and mass to reach a new equilibrium, a process known as fission. The specific mode of this breakup depends critically on the liquid's electrical conductivity. The fission mechanism depends on the comparison between two fundamental lengths: The Drop Diameter: A macroscopic, geometric property of the drop. The Charge Relaxation Length (d_m): A microscopic length scale inherent to the liquid, defined as $d_m = (\gamma\tau^2/\rho)^{1/3}$; Liquid surface tension (γ); electrical relaxation time (τ); and liquid density (ρ). This parameter encapsulates the liquid's ability to redistribute electric charge. It depends on the Electrical Relaxation Time ($\tau = \varepsilon\varepsilon_0/K$) (the characteristic time it takes for charge to move and neutralize imbalances within the liquid). This is the most crucial component, being proportional to liquid dielectric constant (ε) and inversely proportional to the electrical conductivity (K).

S6.2. Field-Enhanced Mechanisms at the Quartz-Water Interface

Strong local electric fields (~10^8 V/m, Figure 4B and C) at curved droplet interfaces accelerate water autoionization via field-induced O-H bond destabilization, enhancing the Grotthuss proton-hopping mechanism. Ab initio molecular dynamics show that electric fields >10^9 V/m reduce water dissociation barriers by orienting hydrogen-bond networks and promoting Eigen-to-Zundel cation transitions, increasing proton availability by orders of magnitude.[5,6] These protons adsorb preferentially at surface silanol defect sites (Si-OH/Si-O^-), which constitute ~5-10% of quartz terminations and serve as reactive gateways for hydrolysis. Ab initio calculations reveal that OH^-/H^+-catalyzed attack on bridging Si-O-Si bonds proceeds via: 1) protonation of

the siloxane bridge oxygen generates a geminal diol intermediate (≡Si–OH···HO–Si≡), with an activation barrier of 4–19 kcal mol^{-1}; 2) formation of a pentacoordinated silicon transition state (activation energy ~90 kJ mol^{-1}), whose barrier is further attenuated under local mechanical stress and 3) asymmetric Si–O bond scission yielding silanol (≡Si–OH) and siloxide ($^{-}$O–Si≡) terminations (ΔE ≈ 300 kJ mol^{-1} in vacuum, substantially lowered by solvation and electro-mechanical coupling).[7,8] Maxwell electrostatic stresses (~562 kPa, Figure S7) arising from field localization generate interfacial pressures of 10–100 MPa, comparable to tectonic stress regimes known to fracture quartz lattices. We note that the range of interfacial pressures mentioned is due to local geometric amplification at droplet protrusions and stress concentration at quartz particle poles. In synergy with H-induced anisotropic lattice slip (preferential weakening of perpendicular Si–O bonds), this establishes a coherent macro-to-micro mechanistic cascade: electrohydrodynamic instabilities (Figure 4) deliver field and stress to silanol-terminated interfaces, where proton-induced chemical stress enables atomic-scale bond cleavage.

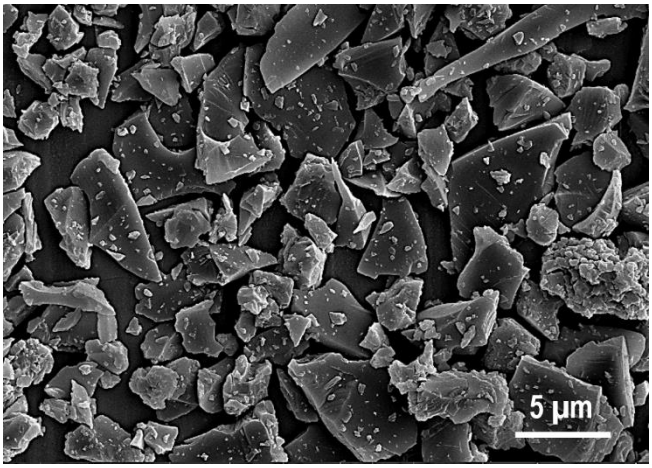

Figure S1. Field-emission scanning electron microscopic (FESEM) image of ground and separated natural quartz used for electrospray, showing particle sizes between 5 and 10 µm. A few smaller particles that are naturally adhered to the micron-sized particles remain attached even after ultrasonication.

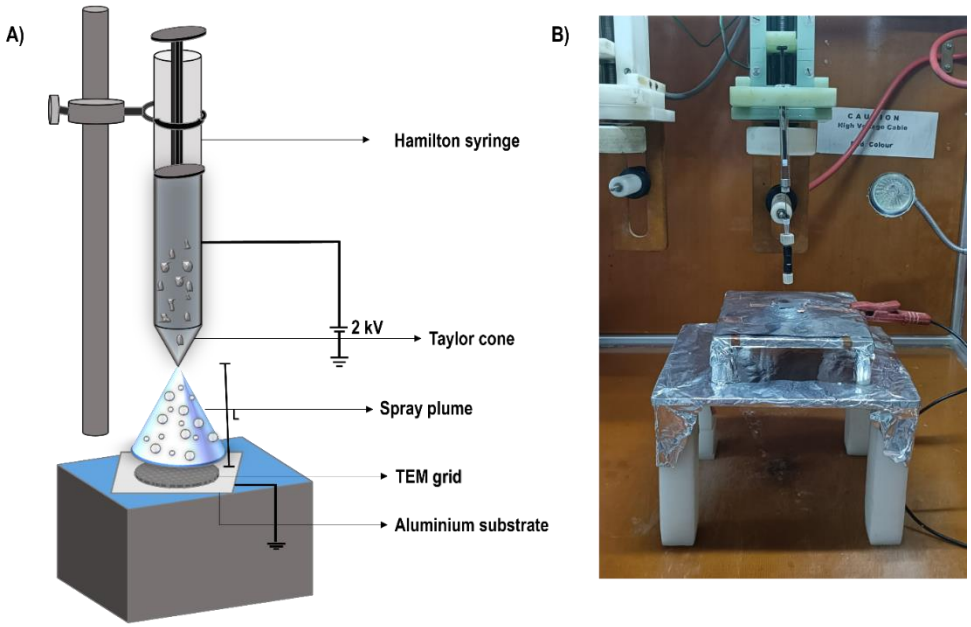

Figure S2. Schematic and photograph of the custom-built electrospray deposition setup. The electrospray was generated using a gas-tight Hamilton syringe connected to a fused silica capillary. A carbon-coated copper TEM grid was placed on the grounded substrate at a tip-to-

substrate distance of 1.5 cm. The visible spray plume confirms stable spray formation during operation. The schematic illustrates the overall configuration of the syringe, high-voltage power supply, and collector geometry used for electrospray deposition of quartz.

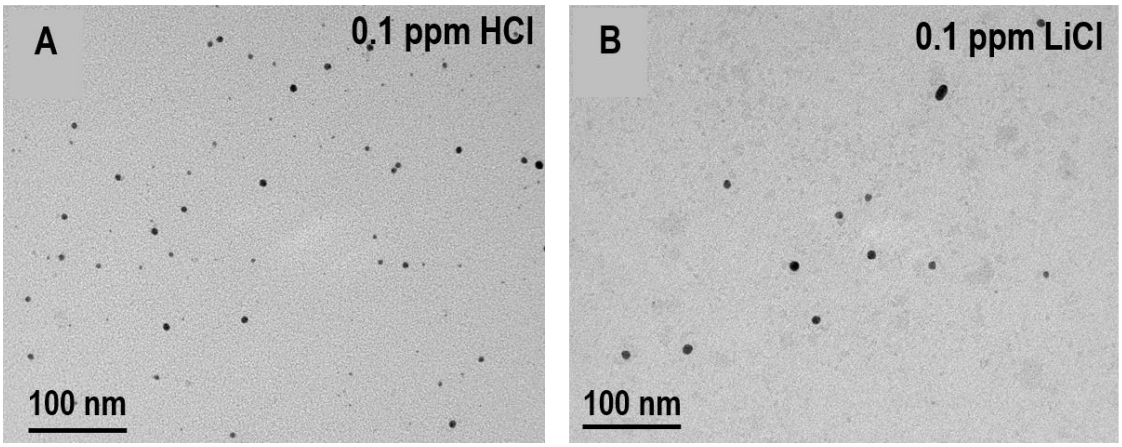

Figure S3. TEM images after electrospray deposition showing disintegration of quartz particles suspended in A) HCl and B) LiCl solutions under an applied potential of 1.5 kV and at a tip-to-substrate distance of 1.5 cm, demonstrating uniform nanoparticle formation facilitated by proton and lithium ion-assisted cleavage.

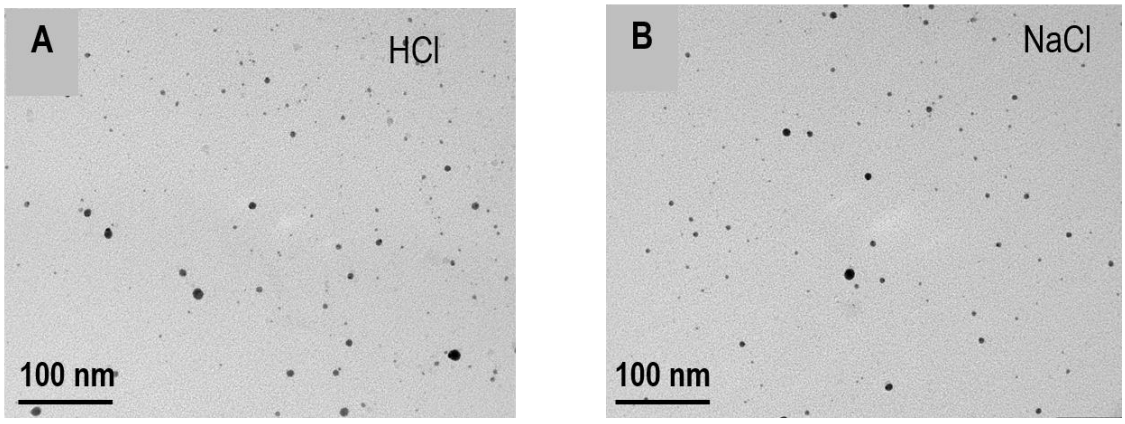

Figure S4. TEM images of quartz nanoparticles synthesized after electrospray deposition of quartz suspended in A) HCl and B) NaCl solutions (1.5 μM each) at an applied potential of 2.0 kV and a tip-to-substrate distance of 1.5 cm.

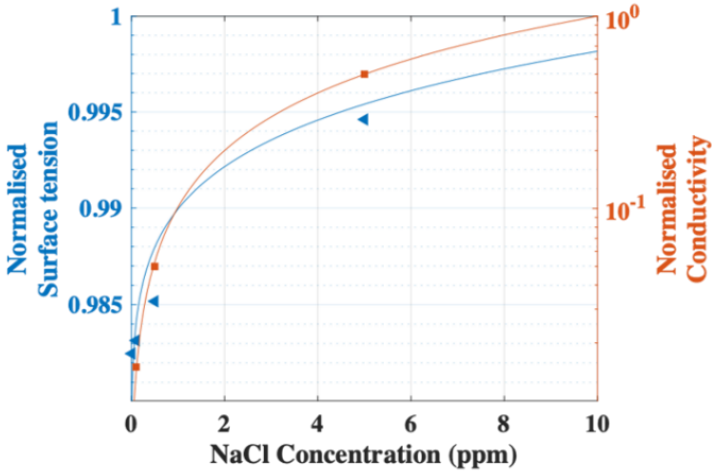

Figure S5. Variation of surface tension and conductivity of aqueous NaCl solutions with concentration, showing that trace ionic impurities (ppm levels) significantly affect electrical conductivity while only slightly influencing surface tension.

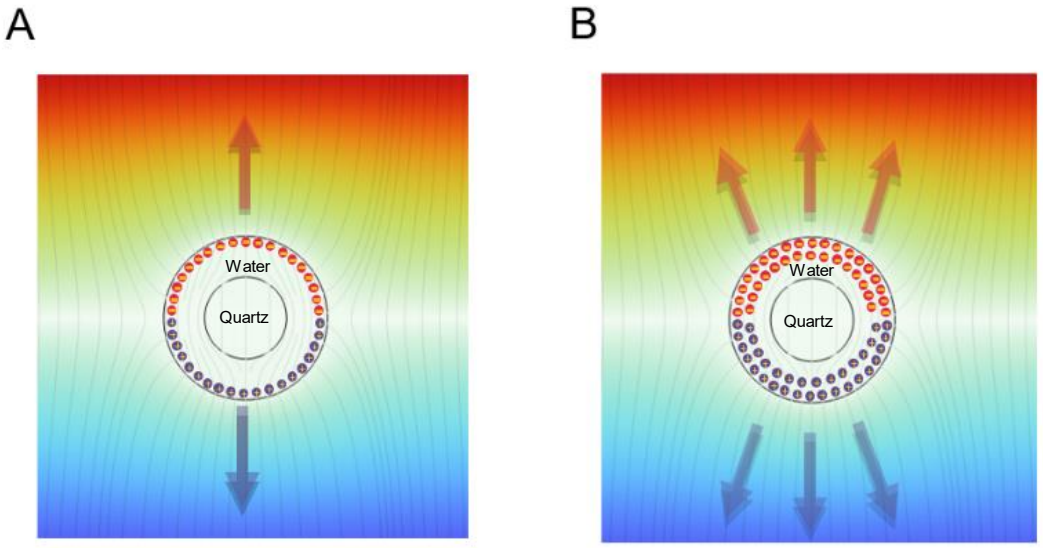

Figure S6. Schematic representation of a A) two-phase droplet system consisting of a solid quartz core ($\varepsilon_r = 4$) surrounded by an aqueous NaCl solution layer ($\varepsilon_r = 80$) suspended in air ($\varepsilon_r = 1$). B) The addition of NaCl enhances surface charge density and outward Coulombic force at the droplet interface.

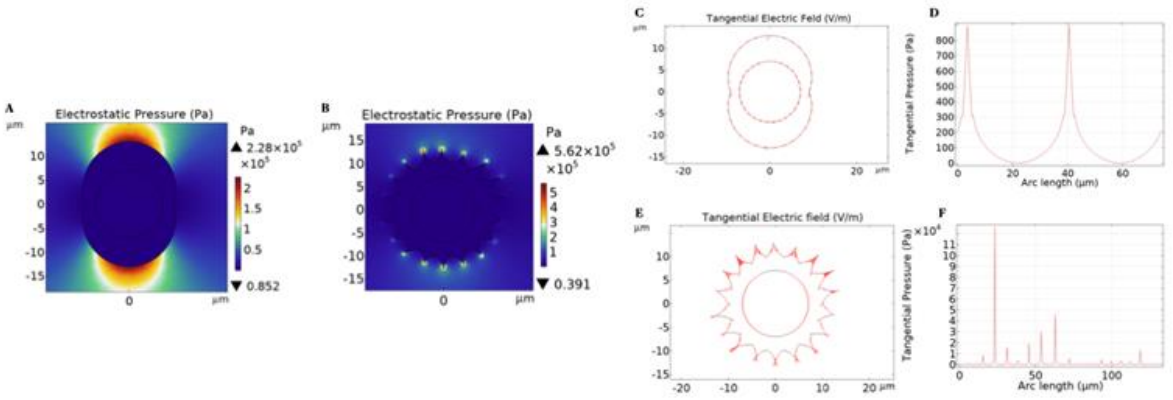

Figure S7. The electrostatic pressure developed on the droplet system is represented in A) and B). The electrostatic pressure developed due to the tangential component of the electric field: C) and D) low salt concentrations, D and F) higher salt concentrations.

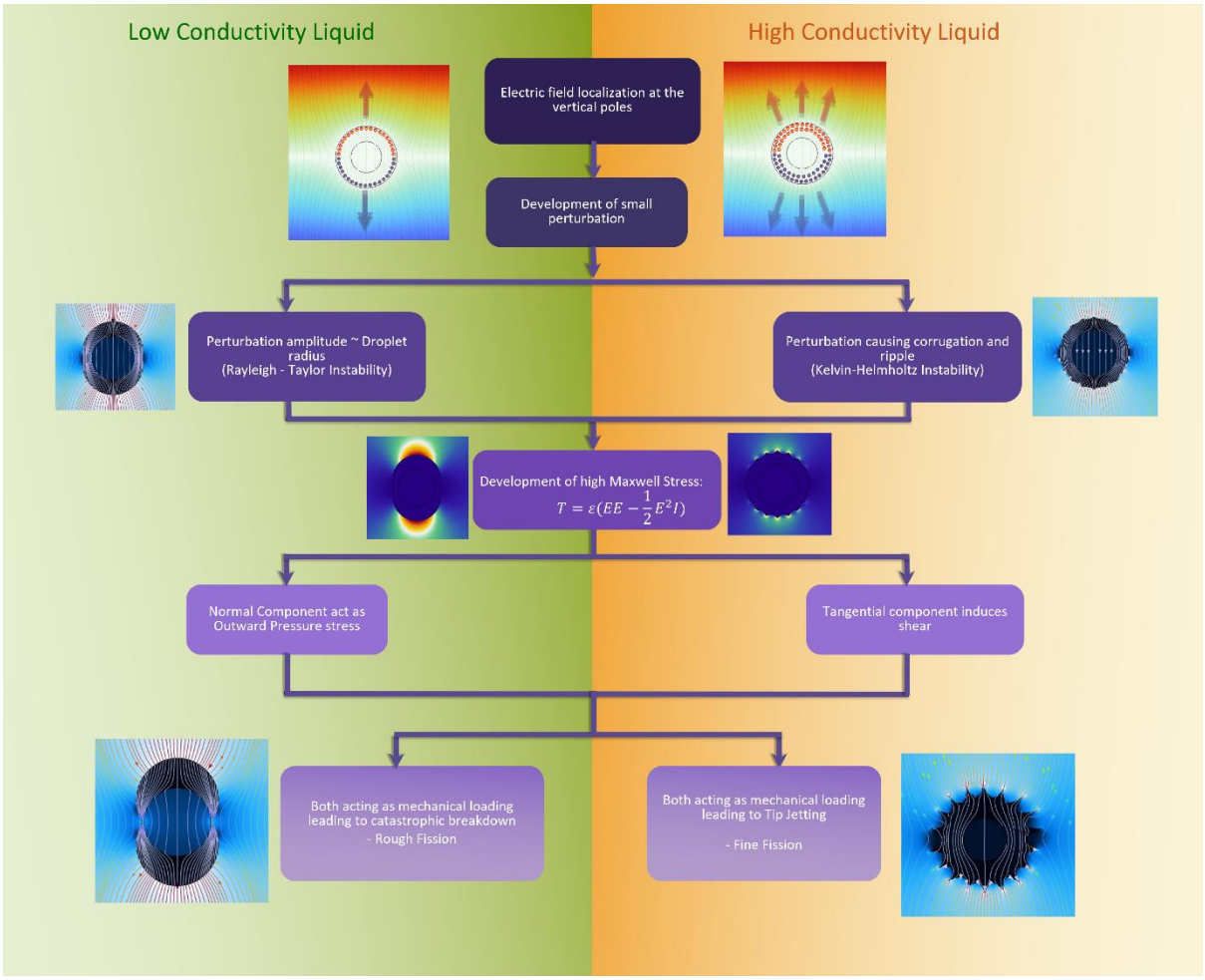

Figure S8. Physical phenomenon, along with the flow diagram underlying the breakup of a quartz particle encapsulated within a salty water–quartz droplet, in varying instability modes, ejected from a high-voltage nozzle.

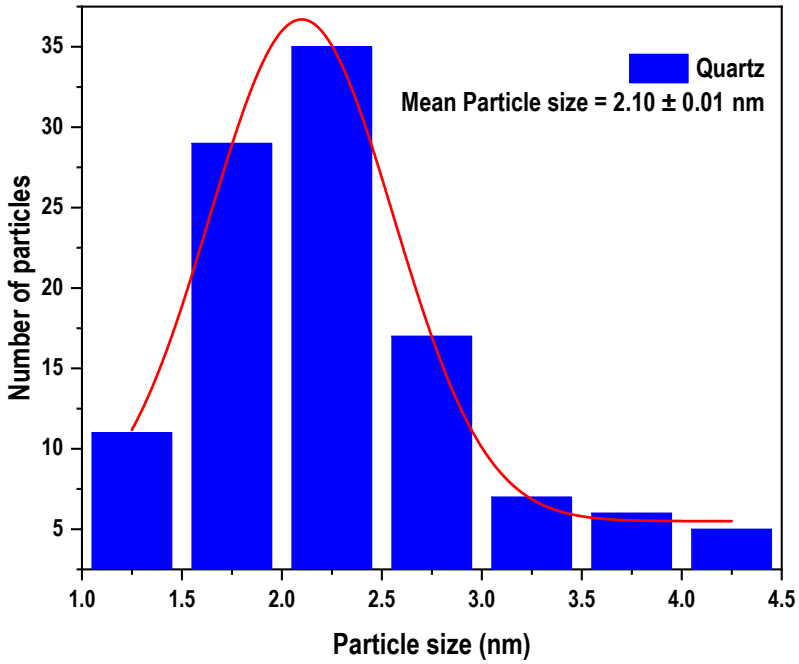

Figure S9. Particle size distribution of nanoparticles of quartz formed by salt-induced electrospray deposition process.

References:

(1) Fernández De La Mora, J. On the Outcome of the Coulombic Fission of a Charged Isolated Drop. Journal of Colloid and Interface Science 1996, 178 (1), 209–218.

(2) Marginean, I.; Znamenskiy, V.; Vertes, A. Charge Reduction in Electrosprays: Slender Nanojets as Intermediates. J. Phys. Chem. B 2006, 110 (12), 6397–6404.

(3) Consta, S. Atomistic Modeling of Jet Formation in Charged Droplets. J. Phys. Chem. B 2022, 126 (41), 8350–8357.

(4) Avadhani, V. S.; Harper, C. C.; Miller, Z. M.; Williams, E. R. Spontaneous Fission of Charged Water Nanodrops: Unveiling the Stochastic Nature of Fission Pathways and Dynamics. J. Am. Chem. Soc. 2025, 147 (22), 18853–18863.

(5) Saitta, A. M.; Saija, F.; Giaquinta, P. V. Ab Initio Molecular Dynamics Study of Dissociation of Water under an Electric Field. *Phys. Rev. Lett.* **2012**, *108* (20), 207801.

(6) Litman, Y.; Michaelides, A. Entropy Governs the Structure and Reactivity of Water Dissociation Under Electric Fields. *J. Am. Chem. Soc.* **2025**, *147* (49), 44885–44894.

(7) Xiao, Y.; Lasaga, A. C. Ab Initio Quantum Mechanical Studies of the Kinetics and Mechanisms of Quartz Dissolution: OH− Catalysis. *Geochim. Cosmochim. Acta* **1996**, *60* (13), 2283–2295.

(8) Wu, B.; Wang, J.; Cao, Y.; Zhou, L.; Sun, S.; Lou, H.; Jiang, X. Dissolution Characteristics at the Quartz–Water Interface in Different Environments: Insights from Molecular Dynamics Simulations. *ACS Omega* **2026**, *11* (5), 7105–7114.